Fld1p, a functional homologue of human seipin, regulates the size of lipid droplets in yeast

Weihua Fei,[1] Guanghou Shui,[1] Bruno Gaeta,[2] Ximing Du,[2] Lars Kuerschner,[3,4] Peng Li,[5] Andrew J. Brown,[2] Markus R. Wenk,[1] Robert G. Parton,[3,4] and Hongyuan Yang[1,2]

[1]Department of Biochemistry, National University of Singapore, Singapore 117597, Republic of Singapore
[2]School of Biotechnology and Biomolecular Sciences, University of New South Wales, Sydney 2052, New South Wales, Australia
[3]Institute for Molecular Bioscience and [4]Centre for Microscopy and Microanalysis, University of Queensland, Brisbane 4072, Australia
[5]Department of Biological Sciences and Biotechnology, Tsinghua University, Beijing 100084, China

Lipid droplets (LDs) are emerging cellular organelles that are of crucial importance in cell biology and human diseases. In this study, we present our screen of ~4,700 *Saccharomyces cerevisiae* mutants for abnormalities in the number and morphology of LDs; we identify 17 *fld* (*few LDs*) and 116 *mld* (*many LDs*) mutants. One of the *fld* mutants (*fld1*) is caused by the deletion of *YLR404W*, a previously uncharacterized open reading frame. Cells lacking *FLD1* contain strikingly enlarged (supersized) LDs, and LDs from *fld1*Δ cells demonstrate significantly enhanced fusion activities both in vivo and in vitro. Interestingly, the expression of human seipin, whose mutant forms are associated with Berardinelli-Seip congenital lipodystrophy and motoneuron disorders, rescues LD-associated defects in *fld1*Δ cells. Lipid profiling reveals alterations in acyl chain compositions of major phospholipids in *fld1*Δ cells. These results suggest that an evolutionally conserved function of seipin in phospholipid metabolism and LD formation may be functionally important in human adipogenesis.

Introduction

Lipid droplets (LDs) are intracellular lipid inclusions consisting primarily of triacylglycerols (TAGs) and sterol esters (SEs; Murphy and Vance, 1999). Recent studies have proven that LDs are dynamic intracellular organelles that are functionally connected with other cellular compartments (for review see Martin and Parton, 2006). LDs from different cell types are bounded by a monolayer of phospholipids and characterized by unique surface proteins, which may contribute to the biogenesis, maturation, and stability of LDs (Martin and Parton 2006; Wolins et al., 2006). LDs are believed to originate from microdomains of the ER, where enzymes for the synthesis of neutral lipids reside. Newly synthesized neutral lipids are thought to accumulate between two leaflets of the ER bilayer before budding into the cytosol (Martin and Parton 2006; Wolins et al., 2006). With the assistance of microtubules, nascent LDs appear to fuse with each other until a certain size is reached (Bostrom et al., 2005). A recent study identified SNARE proteins as part of the core machinery for the fusion of LDs (Bostrom et al., 2007). Despite recent progress, many fundamental questions remain. For instance, how is the fusion process regulated, and what factors determine the final size of a mature LD?

Correspondence to Hongyuan Yang: h.rob.yang@unsw.edu.au

Abbreviations used in this paper: BSCL, Berardinelli-Seip congenital lipodystrophy; CGL, congenital generalized lipodystrophy; LD, lipid droplet; MRM, multiple reaction monitoring; PA, phosphatidic acid; SC, synthetic complete; SE, sterol ester; TAG, triacylglycerol; TEM, transmission EM.

The online version of this article contains supplemental material.

Results and discussion

In an effort to identify novel gene products that may play a role in LD formation, Nile red, a vital dye specific for intracellular LDs, was used to visually screen the entire collection of viable single-gene deletion mutants of the budding yeast *Saccharomyces cerevisiae* for abnormalities in the number and morphology of LDs (Greenspan et al., 1985). Because the number and morphology of LDs may vary depending on growth phases, wild-type cells and all mutants were grown overnight to stationary phase (OD_{600} = ~5) in this study immediately followed by Nile red staining and fluorescence microcopy. Wild-type cells at stationary phase showed 5.16 ± 2.18 LDs per cell on average (±SD; n = 200), and ~80% of the cells displayed three to seven LDs (Fig. 1 A, a). To simplify the screening process, we arbitrarily categorized deletion strains with the majority (>80%) of cells accumulating on average less than three LDs as *fld* (*few LDs*) mutants and strains accumulating more than seven LDs as *mld* (*many LDs*) mutants. Among the *mld* mutants, strains containing >11 LDs were classified as strong *mld* mutants. We isolated

The Journal of Cell Biology, Vol. 180, No. 3, February 11, 2008 473–482
http://www.jcb.org/cgi/doi/10.1083/jcb.200711136

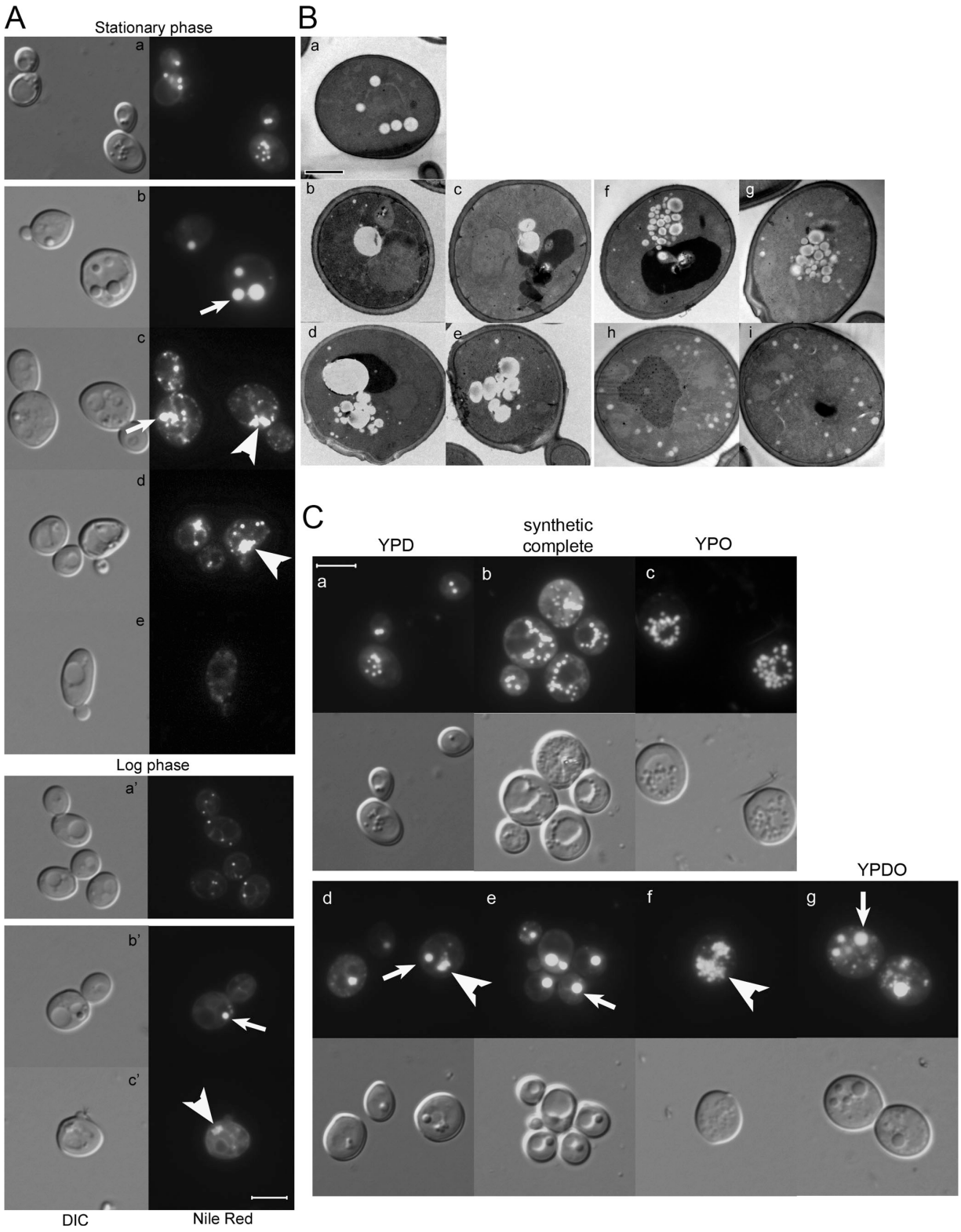

Figure 1. **The *fld1Δ (ylr404wΔ)* cells synthesize morphologically distinct LDs.** (A) Both wild-type and *fld1Δ* cells were grown in YPD medium until stationary phase or until log phase. Cells were stained with 20 μg/ml Nile red and immediately observed for LDs under a fluorescence microscope. Micrographs of the wild-type cells (a and a′) and *fld1Δ* cells (b–e, b′, and c′) are shown. Supersized LDs (b, c, and b′) are indicated by arrows, and aggregation of LDs (c, d, and c′) is indicated by arrowheads. DIC, differential interference contrast. (B) Conventional TEM of wild-type and *fld1Δ* cells. Cells were grown in YPD to stationary phase, fixed with 2.5% (vol/vol) glutaraldehyde and 2% (wt/vol) osmium tetroxide, and subjected to EM. LDs are seen as electron-transparent droplets. TEM of wild-type (a) and *fld1Δ* (b–i) cells. (C) Culture media affect LD morphology in *fld1Δ* cells. Wild-type and *fld1Δ* cells were grown until stationary phase in YPD medium (a and d), SC medium (b and e), YPO (oleate) medium (c and f), or YPDO medium (g). The preparation of media was described in Materials and methods. Nile red staining of wild-type (a–c) and *fld1Δ* (d–g) cells. Arrows indicate supersized LDs, and arrowheads indicate aggregated LDs. Bars: (A and C) 5 μm; (B) 1 μm.

17 *fld* mutants and 116 *mld* mutants (Tables S1 and S2, available at http://www.jcb.org/cgi/content/full/jcb.200711136/DC1).

We focused on *FLD1*, which corresponds to a previously uncharacterized ORF, *YLR404W*, because its deletion not only affected the number of LDs but also gave rise to strikingly enlarged or aggregated LDs (Fig. 1). When grown in rich medium until stationary phase, wild-type cells usually display three to seven LDs under the microscope. The LDs were between 0.2 and 0.4 μm in diameter and were almost spherical in shape (Fig. 1 A, a). In contrast, LDs observed in *fld1Δ* cells were very irregular in terms of quantity, shape, and size. Up to 30% of the total population of *fld1Δ* cells contained one or a few supersized LDs that were spherical in shape and were about 0.5–1.5 μm in diameter (Fig. 1 A, b; arrow), which means that the volume of the largest LD of the *fld1Δ* cells was about 50 times that of the largest LD found in wild-type cells. About 60% of the *fld1Δ* population contained an amorphous aggregation of neutral lipids in addition to several small LDs (Fig. 1 A, c and d; arrowheads). The remaining ∼10% of the *fld1Δ* cells contained scattered and weakly stained LDs, which had diameters of <0.1 μm (Fig. 1 A, e). The phenotypic characteristics of *fld1Δ* were also observed in log-phase cells. When grown to log phase (OD_{600} = 0.8), most of the wild-type cells contained two or three LDs that were slightly smaller than those of stationary-phase cells (Fig. 1 A, a′). The LDs in *fld1Δ* at log phase show similar morphology to cells grown to stationary phase except that the supersized LDs and the aggregation of neutral lipids were smaller and more weakly stained (Fig. 1 A, b′ and c′; arrow and arrowhead, respectively).

To examine the ultrastructure of *fld1Δ* cells, we performed transmission EM (TEM) of the wild-type and *fld1Δ* strains. Cells were grown in rich medium until stationary phase and were subjected to TEM analysis. One typical cross section of a wild-type cell contained five LD profiles, which were round and about 0.2–0.4 μm in diameter (Fig. 1 B, a). The cross sections of *fld1Δ* mutant cells again showed three classes of LDs with distinct morphologies. Up to 30% of cells displayed one or a few supersized LDs per section, which were either round or oval (Fig. 1 B, b–d). Consistent with the result of fluorescence microscopy, the diameters of some LDs were up to 1.5 μm (Fig. 1 B, d). Aggregated LDs were found in ∼60% of the mutant population (Fig. 1 B, d–g). These aggregations were reminiscent of the amorphous neutral lipid clump observed under fluorescence microscopy (Fig. 1 A, c and d). The rest of the *fld1Δ* cells (∼10% of the total population) contained many tiny LDs, most of which had a diameter of <0.1 μm and were loosely scattered (Fig. 1 B, h and i).

Yeast cells undergo marked proliferation of LDs when they are grown in defined medium (synthetic complete [SC]) or in an oleate-based medium (YPO [YP plus oleate, no glucose]; Binns et al., 2006). As shown in Fig. 1 C (a–c), a great increase in the number of LDs was observed in wild-type cells grown in SC or YPO media. When *fld1Δ* cells were grown in YPD, the majority (∼70%) of the cells showed amorphous aggregations of many intermediate-sized LDs (Fig. 1 B, f and g). In contrast, >70% of the *fld1Δ* cells displayed only one or two supersized LDs when cultured in SC media (Fig. 1 C, e). Moreover, amorphous aggregation of many small LDs that were common in cells cultured in YPD media were only observed in about 10% of the cells grown in SC. Interestingly, when *fld1Δ* cells were cultured in YPO medium, >95% (191/200 cells examined) of the cells displayed amorphous aggregations of LDs without the supersized LDs (Fig. 1 C, f). However, when *fld1Δ* cells were cultured in YPDO medium (YPD + oleate), the large LDs appeared again together with the aggregation of smaller LDs (Fig. 1 C, g). Thus, we identified a commonly used growth medium (SC) that allowed us to easily distinguish wild-type and *fld1Δ* cells based on the presence or absence of supersized LDs (Fig. 1 C, compare b with e).

We measured the steady-state levels of TAG and SE as well as the rate of oleate incorporation into TAG and SE (Oelkers et al., 2002). For cells grown in YPD to log phase, the deletion of *FLD1* caused about a doubling in the steady-state levels of both TAG and SE (Fig. S1 A, available at http://www.jcb.org/cgi/content/full/jcb.200711136/DC1). The rate of SE synthesis was also upregulated by 70% in *fld1Δ* deletion cells, but little difference in the rate of oleate incorporation into TAG was observed (Fig. S1 B). Similar patterns of changes were detected for cells grown in YPD to stationary phase or in SC to either log or stationary phase (unpublished data).

The expression of *FLD1-GFP* in *fld1Δ* cells restored the normal morphology of LDs (Fig. 2, A and B). We performed a series of subcellular fractionation experiments to analyze the cellular distribution of Fld1p. Cell extracts prepared from the *fld1Δ* strain expressing Fld1-GFP were fractionated by centrifugation at 13,000 *g* for 10 min, resulting in P13 pellet and S13 supernatant fractions that were probed with antibodies against GFP and Dpm1p, an ER marker. Both Fld1p and Dpm1p were found in the P13 fraction, which contains large membranous structures such as the vacuole, ER, and plasma membrane (Fig. 2 C). The same cell extracts were subjected to continuous sucrose density gradient analysis. 13 fractions were collected from top to bottom (1–13) and were probed for the presence of GFP and Dpm1p by immunoblotting. Dpm1p and Fld1p appeared to exist in the same density fractions (Fig. 2 D). Localization of Fld1-GFP was also examined in live cells by fluorescent microscopy, and Fld1-GFP was found in both perinuclear and peripheral ER (Fig. 2 E). Finally, immuno-EM was used to pinpoint the exact location of Fld1p. Fld1p-GFP was found to be associated with the cortical ER and the nuclear envelope, which is consistent with the putative ER localization observed by light microscopy. In addition, labeling was observed throughout the ER, including regions in contact with LDs (Fig. 2 F).

The existence of morphologically distinct LDs within *fld1Δ* suggests enhanced fusion activities of LDs: the small, discrete LDs may represent the newly synthesized LDs, which tend to aggregate before eventually fusing into a supersized LD. To test this hypothesis, wild-type and *fld1Δ* cells were cultured in SC medium until midlog phase (OD_{600} = ∼1.0), stained with Nile red, and observed for the fusion of LDs by fluorescent microscopy. Cells in which two or several LDs lay close together were targeted. We examined 200 cases of adjacent LDs each for mutant and wild-type cells and monitored every case for 1 min. The criteria we used to define fusion were described previously (Bostrom et al., 2007). No fusion events were observed in wild-type cells, but

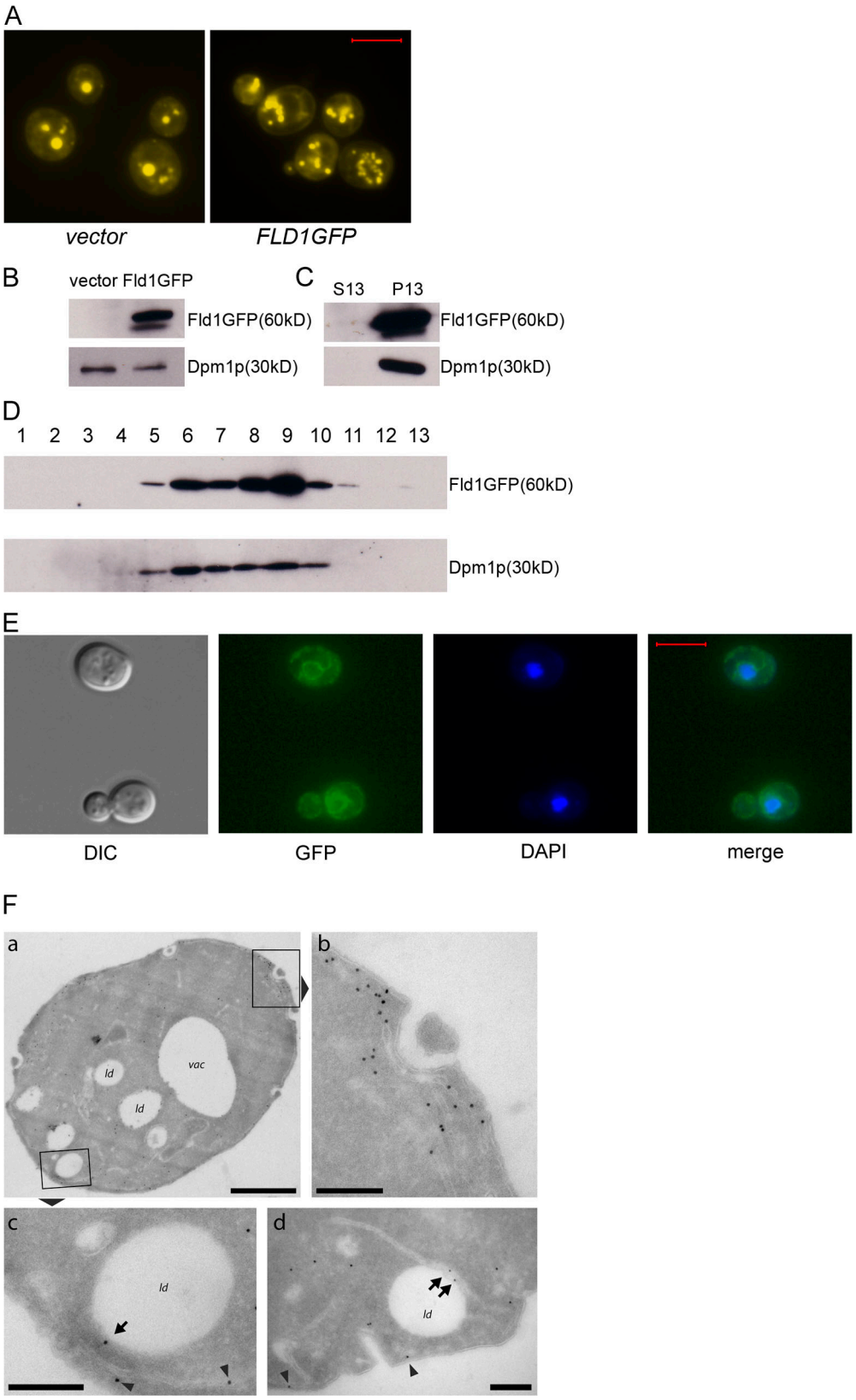

Figure 2. **Fld1p localizes predominantly to the ER.** (A) The expression of *FLD1-GFP* complements the *fld1Δ* phenotype. Cells were transformed either with *YCplac111* vector alone or with *YCplac111-FLD1-GFP* and grown in SC media without leucine. (B) *fld1Δ* cells transformed either with *YCplac111* vector alone or with *YCplac111-FLD1-GFP* were lysed and immunoblotted with anti-GFP or Dpm1p antisera. (C) Cells expressing Fld1-GFP were spheroplasted and subjected to differential centrifugation as described in Materials and methods. The 13,000-*g* pellet (P13) and soluble fraction (S13) were analyzed by SDS-PAGE and immunoblotting. (D) Cell lysates were loaded on the top of a continuous sucrose gradient (10–53%) and centrifuged at 100,000 *g* for 15 h. Fractions were collected from the top, separated by SDS-PAGE, and immunoblotted with antisera against GFP or Dpm1. (E) Fluorescence microscopy

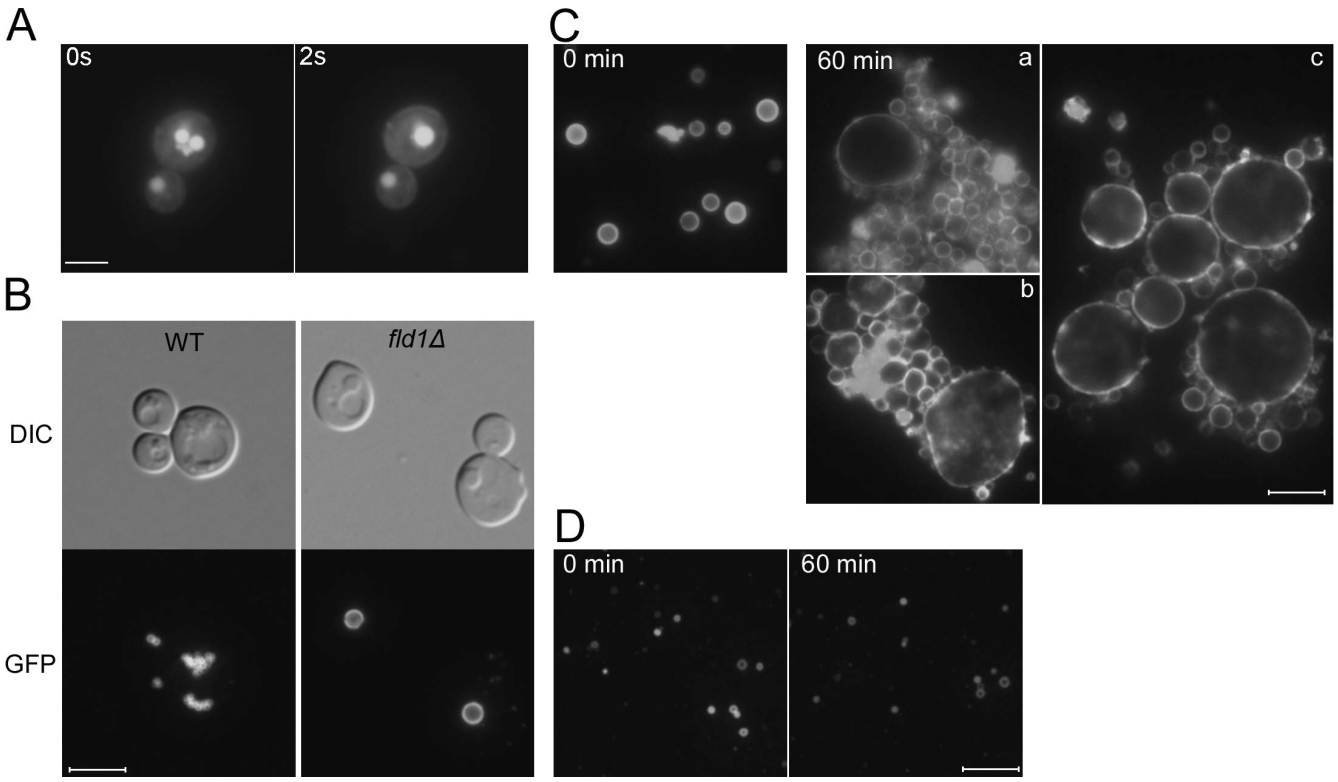

Figure 3. **LDs from *fld1Δ* cells demonstrate enhanced fusion activity in vivo and in vitro.** (A) *fld1Δ* cells were grown in SC medium until midlog phase (OD_{600} = ~1) and were stained with Nile red. Cells in which two or several LDs lay close together were targeted. Images were collected at 2-s intervals. (B) Tgl3p-GFP localizes to LDs both in wild-type (WT) and *fld1Δ* strains. DIC, differential interference contrast. (C) Tgl3p-GFP–tagged LDs were isolated from *fld1Δ* cells grown in SC media, resuspended in PBS, and left for gentle shaking at 30°C for 1 h. The images were taken before (0 min) and after incubation (60 min; a–c). (a–c) Three typical results. (D) LDs isolated from wild-type cells grown in SC media do not fuse under the same conditions as described in C. Bars, 5 μm.

fusion was detectable for about 10% (19/200) of all mutant cases. As shown in Fig. 3 A, two closely positioned LDs appeared to completely fuse within a span of 2 s. The size of the newly formed LD appeared to be the combined size of the two parent LDs.

To further demonstrate enhanced LD fusion in *fld1Δ* cells, we isolated LDs from wild-type and mutant cells both carrying Tgl3p-GFP. Tgl3p is a triglyceride lipase that localizes to the surface of LDs (Fig. 3 B; Athenstaedt and Daum, 2003). Purified LDs from both wild-type and *fld1Δ* cells were left in PBS buffer and examined by microscopy before and after 60 min. Whereas LDs from wild-type cells remained scattered and unchanged in size, LDs from *fld1Δ* cells formed aggregates or fused into huge lipid inclusions reminiscent of the supersized LDs observed in live *fld1Δ* cells (Fig. 3, C and D). The lipid inclusions observed in vitro are much larger than the supersized LDs in live cells (~5 μm vs. ~1 μm in diameter), suggesting that additional fusion events occurred in vitro.

Remote homology detection techniques were used to look for a mammalian homologue to Fld1p. Human seipin, a protein associated with Berardinelli-Seip congenital lipodystrophy (BSCL) and motorneuron disorders, was identified (Agarwal and Garg, 2004). Seipin shows weak sequence conservations to Fld1p, but they both contain two predicted transmembrane domains, and their predicted secondary structures are also very similar (Fig. 4 A). Human seipin is encoded by the *BSCL2* gene, which gives rise to at least three different mRNAs and two peptides with 398 or 462 amino acids (Lundin et al., 2006). The region that covers the first 280 amino acids of human seipin is 88% identical among rat, mouse, chimpanzee, and human homologues (Agarwal and Garg, 2004). This is interesting because all of the sequence conservations between yeast Fld1p (285 amino acids) and seipin fall within this region. To test whether seipin is a functional homologue of Fld1p, full-length human and mouse seipin homologues were expressed in *fld1Δ* cells grown in SC media. The average diameter of the LDs is 1.27 ± 0.19 μm (n = 117) without human seipin and 0.43 ± 0.05 μm (n = 106) with seipin (Fig. 4 B). We also examined the effects of point mutations in seipin that are implicated in lipodystrophy (A212P) and motoneuron disorders (N88S and S90L). The expression of N88S and S90L but not A212P rescued the defects in LD morphology (Fig. 4 C).

of cells expressing Fld1-GFP. DIC, differential interference contrast. (F) Localization of Fld1p by immuno-EM. Cells were grown in SC media to late log phase, fixed, and processed for immuno-EM with antisera against GFP. (a) An overview of a representative cell. (b) High magnification image depicting immunoreactivity at the cortical ER. (c and d) High magnification images depicting immunoreactivity at the cortical ER (arrowheads) and in close proximity to LDs (arrows). Vac, vacuole; ld, lipid droplet. Bars: (A and E) 5 μm; (F, a) 1 μm; (F, b–d) 200 nm.

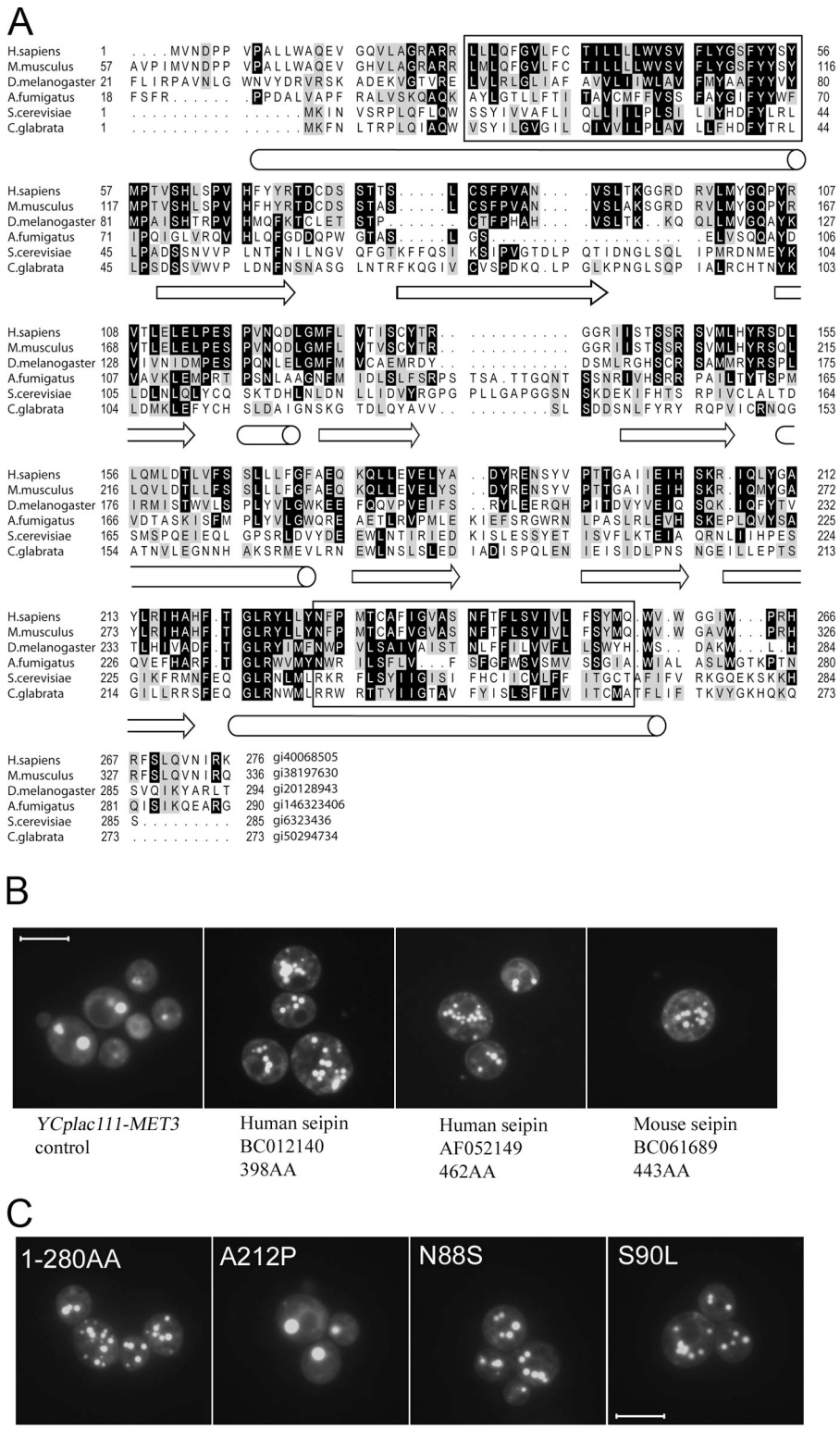

Figure 4. **Expression of human and mouse *BSCL2* (seipin) rescues defects in LD morphology in *fld1Δ* cells.** (A) Sequence alignment of seipin homologues with gene identification numbers. The alignment was created using the PRALINE server (Simossis and Heringa, 2005). Identical amino acids among seipin homologues are shaded in black, and similar residues are shaded in gray. The secondary structures predicted by PSIPRED (position-specific iterated predication of protein secondary structure) through the Ali2D server (http://toolkit.tuebingen.mpg.de/ali2d) are indicated below the sequences. The boxed regions are the two transmembrane domains predicted through the PSIPRED server (McGuffin et al., 2000). (B and C) The expression of seipin in yeast. *fld1Δ* strains transformed with *YCplac111-MET3-BSCL2*–expressing full-length seipins (human BC012140 and AF052149 and mouse BC061689), human seipin (BC012140) amino acid residues 1–280, seipin mutants, or the vector alone were grown in SC media minus leucine to stationary phase followed by Nile red staining and fluorescence microscopy. Bars, 5 μm.

This is not surprising because A212P is considered a loss-of-function mutation, whereas N88S and S90L may represent gain-of-function mutations (Windpassinger et al., 2004). Lastly, expression of the highly conserved 280–amino acid region of seipin rescued the defects in LD morphology (Fig. 4 C). Together, these results strongly suggest that human seipin represents the functional homologue of Fld1p.

Congenital generalized lipodystrophy (CGL; or BSCL) is an autosomal recessive disorder that is characterized by the almost complete absence of adipose tissue and severe insulin resistance (Agarwal and Garg, 2004). Genome-wide linkage analysis identified two loci for CGL: CGL type 1 (CGL1) is caused by mutations in the AGPAT2 (1-acylglycerol-3-phosphate-*O*-acyl transferase 2) gene, and CGL2 is caused by mutations in *BSCL2*,

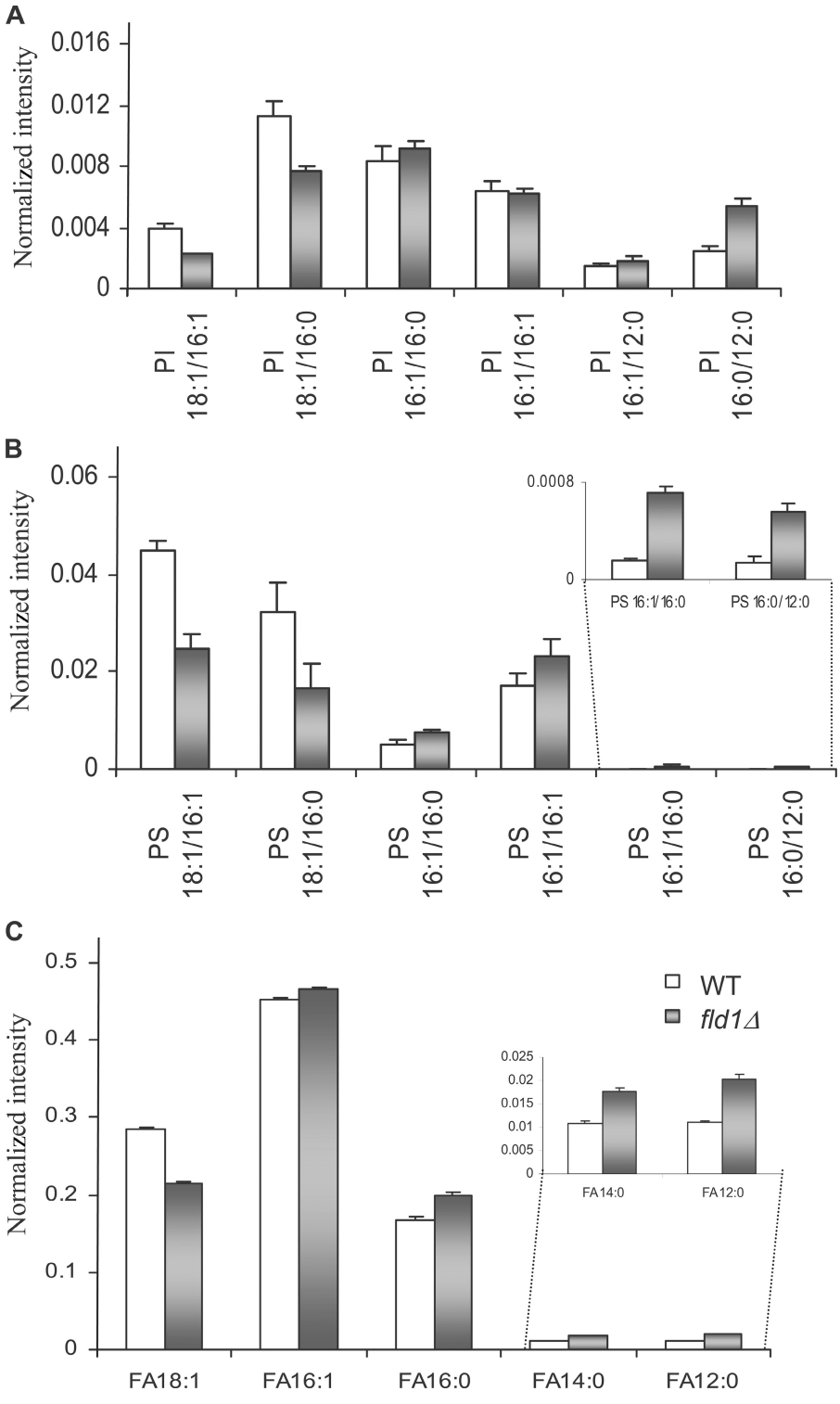

Figure 5. **Mass spectrometry analysis of glycerophospholipids.** (A and B) Wild-type and *fld1*Δ cells were grown to stationary phase in SC media. Total lipids were extracted and analyzed by high performance liquid chromatography/mass spectrometry. The results for phosphatidylinositol (PI) and phosphatidylserine (PS) are shown in A and B, respectively. Data for phosphatidylethanolamine and phosphatidylcholine are shown in Fig. S3 (available at http://www.jcb.org/cgi/content/full/jcb.200711136/DC1). Data are represented as normalized intensities based on a formula described in Materials and methods. (C) Fatty acyl (FA) profiles of polar lipids. The y axis represents the normalized values of each fatty acyl to the sum of intensities of all fatty acyls. $n = 4$; values are means ± SD (error bars).

which encodes seipin (Magre et al., 2001; Agarwal et al., 2002). AGPAT2 catalyzes the formation of phosphatidic acid (PA), but knocking down AGPAT2 led to elevated levels of several phospholipid species, including PA, and to a delay in the activation of key transcription factors for adipogenesis such as C/EBPβ and PPARγ (Gale et al., 2006). Therefore, AGPAT2 controls adipogenesis through modulation of the synthesis of phospholipids. In contrast, little is known about the role of seipin in adipogenesis and lipodystrophy. Because mutations in AGPAT2 and BSCL2 cause similar clinical manifestations, we wondered whether aberrant phospholipid metabolism may underlie the cellular defects for both conditions. Lipid species from wild-type and *fld1Δ* whole cell extracts were analyzed by electrospray ionization tandem mass spectrometry. The level of PA increased slightly in *fld1Δ* cells (unpublished data). Interestingly, there is a shift from long-chain (18:1) to medium/short-chain (16:0, 14:0, and 12:0)

fatty acid incorporation into all major phospholipids as a result of the deletion of *FLD1* (Fig. 5 and Fig. S3, available at http://www.jcb.org/cgi/content/full/jcb.200711136/DC1).

We identified seipin (Fld1p) as a novel regulator of the cellular dynamics of LDs. The deletion of *FLD1* causes increased levels of neutral lipids, clustering of LDs, and formation of enlarged (supersized) LDs. Increased neutral lipids often lead to an increase in the number but not the size of LDs (Fig. 1, C, b and c; and Fig. S2, available at http://www.jcb.org/cgi/content/full/jcb.200711136/DC1). Therefore, the appearance of supersized LDs in *fld1Δ* cells is unlikely to be caused by an increase in neutral lipids. Rather, the physical property of the surface of LDs might have been altered in *fld1Δ* cells as a result of changes in phospholipids, which may facilitate the clustering and fusion of LDs. In support of this, LDs isolated from *fld1Δ* cells can aggregate and fuse without the supply of ATP and cytoplasmic proteins (Fig. 3 C).

What is the molecular function of Fld1p or seipin? We favor a role of Fld1p in phospholipid/fatty acid metabolism for the following reasons: (1) a shift from long to medium/short acyl chains was detected in *fld1Δ* cells (Fig. 5); (2) LDs isolated from *fld1Δ* cells can aggregate and fuse without the supply of ATP and cytoplasmic proteins, suggesting a role for phospholipids (Fig. 3); (3) the other gene that is associated with CGL is APGAT2, a major enzyme in phospholipid metabolism; and (4) lipin, another well-known protein that is associated with lipodystrophy in mice, is a phosphatidate phosphatase (Han et al., 2006). Deletion of *SPO7* or *NEM1*, two genes involved in the activation of lipin, also caused aberrant LD morphology (Table S1 and our unpublished data).

Results described herein show for the first time that seipin and its homologues modulate the formation and especially fusion of the LDs. Our data also suggest that changes in phospholipid metabolism may be the unifying theme for both CGL1 and CGL2. Understanding the molecular function of seipin will provide mechanistic insights into LD formation and adipogenesis.

Materials and methods

Strains

Both wild-type BY4741 (*MATa his3Δ1 leu2Δ0 met15Δ0 ura3Δ0*) and single deletion mutants, including the *ylr404wΔ* strain (*MATa his3Δ1 leu2Δ0 met15Δ0 ura3Δ0 YLR404W::KanMX4*), were obtained from the European *Saccharomyces cerevisiae* Archives for Functional Analysis collection (Winzeler et al., 1999).

Reagents

Nile red, oleic acid, and Brij58 were purchased from Sigma-Aldrich; glutaraldehyde and osmium tetroxide were obtained from Electron Microscopy Sciences. DAPI, anti-Dpm1 mouse monoclonal, and anti-GFP rabbit polyclonal were purchased from Invitrogen. [4-^{14}C]cholesterol, Ficoll PM400, and [9, 10(n)-^{3}H]oleic acid were purchased from GE Healthcare.

Media

Unless otherwise stated, yeast cells were grown with rotary shaking at 30°C in liquid YPD medium (1% yeast extract, 2% bacto peptone, and 2% dextrose). Alternatively, cells were grown in SC medium (0.67% nitrogen base and 2% dextrose with all amino acids supplemented), YPO medium (1% yeast extract, 2% bacto peptone, and 0.1% oleic acid in 1% Brij58), or in YPDO medium (1% yeast extract, 2% bacto peptone, 2% dextrose, and 0.1% oleic acid in 1% Brij58). Plasmid-carrying strains were grown on synthetic medium with appropriate selection as described previously (Kaiser et al., 1994).

Fluorescence microscopy

Fluorescence imaging was performed on a microscope (DMLB; Leica) with a fluorescent lamp (ebq 100; Curtis). Samples were viewed using a 100× NA 1.30 oil immersion objective lens (Leica). Images were taken with a digital camera (DFC480; Leica) and FW4000 software (Leica).

LD staining

Nile red (Sigma-Aldrich) is a specific and excellent vital dye for intracellular LDs. A 450–490-nm bandpass excitation filter, a 510-nm dichromatic mirror, and a 515-nm longpass emission filter (filter cube I3; Leica) were chosen to view LDs.

Visualization of LD fusion

To record the process of LD fusion in the *fld1Δ* mutant, 3 μl of late log-phase cells (OD_{600} = ~1) stained with Nile red were spotted on a slide and covered with a coverslip. Under the microscope, cells in which two or several LDs lay close together were targeted. Images were collected at 2-s intervals.

GFP

GFP signal was visualized with a 470/40-nm bandpass excitation filter, a 500-nm dichromatic mirror, and a 525/50-nm bandpass emission filter (filter cube GFP; Leica).

DAPI staining of nucleus

Cells fixed with 3.7% formaldehyde for 15 min were stained with 5 μg/ml DAPI. DAPI fluorescence was observed with a 340–380-nm bandpass excitation filter, a 400-nm dichromatic mirror, and a 425-nm longpass emission filter (filter cube A; Leica).

TEM

Cells were grown in rich medium until stationary phase, harvested, fixed with 2.5% glutaraldehyde, and postfixed with 2% (wt/vol) osmium tetroxide. The samples were subsequently dehydrated in a series of graded ethanol and embedded in Spurr's resin. 80-nm ultrathin sections were stained with uranyl acetate and lead citrate and examined under an electron microscope (JEM-1230; JEOL).

Immuno-EM

Immuno-EM of ultrathin cryosections was performed essentially as described previously (Martin et al., 2005). In brief, *fld1Δ* cells transformed with *FLD1-GFP* were grown in SC media to late log phase and fixed in 2% PFA/0.2% glutaraldehyde in 0.1 M PHEM buffer (60 mM Pipes, 25 mM Hepes, 2 mM $MgCl_2$, and 10 mM EGTA), pH 6.9, for 1 h at room temperature. Cells were embedded in 10% gelatin, cryoprotected using polyvinyl pyrrolidone–sucrose, and snap frozen onto specimen holders in liquid N_2. Ultracryomicrotomy was performed by a slight modification of the Tokuyasu technique, and sections were picked up with a 1:1 mixture of 2.3 M sucrose and 2% methyl cellulose. Grids were viewed using a transmission electron microscope (model 1010; JEOL).

DNA manipulations

Construction of a vector expressing GFP-tagged YLR404wp. A 1.4-kb fragment containing the native promoter and the coding sequence before the stop codon of *YLR404W* was amplified by PCR using a 5′ primer (5′-HindIII-TTACCATGCACGTTGTCG) and a 3′ primer (5′-BamHI-GCTATGTTTCTTGGATT). This fragment was then subcloned into the HindIII- and BamHI-cleaved YCplac111-GFP plasmid, in which the GFP coding sequence was inserted between the BamHI and EcoRI restriction sites. A sequence encoding yeast codon bias GFP (yEGFP; a gift from B. Winsor, Université Louis Pasteur, Strasbourg, France) was used for all GFP constructs.

Construction of a vector expressing GFP-tagged Tgl3p. A 2.7-kb fragment containing the natural promoter and the coding sequence before the stop codon of *TGL3* was amplified by PCR using a 5′ primer (5′-ACGGC-HindIII-TCTGTT) and a 3′ primer (5′-BamHI-CCTACTCCGTCTTGCTCTT). This fragment was then subcloned into the HindIII- and BamHI-cleaved YCplac111-GFP plasmid, in which the GFP coding sequence was inserted between the BamHI and EcoRI restriction sites.

Construction of vectors expressing seipins. The coding sequences of human seipin and mouse seipin were amplified by PCR using a 5′ primer (5′-SphI-ATGGTCAACGACCCTCCAGTACCTGC) and a 3′ primer (5′-BamHI-TCAGGAACTAGAGCAGGTGGGGCGCTG) from human cDNA BC012140, a 5′ primer (5′-SphI-ATGTCTACAGAAAAGGTAGACCAAAAGG) and a 3′ primer (5′-BamHI-TCAGGAACTAGAGCAGGTGGGGCGCTG) from human cDNA AF052149, and a 5′ primer (5′-SphI-ATGATACATCAAAGAAGAGAAGCTGG) and a 3′ primer (5′-XbaI-TCAGGAACTGGAGCAGGTCGGGCGTTG)

from mouse cDNA BC061689. The gene sequence encoding the first 280 amino acids of seipin was amplified using a 5′ primer (5′-SphI-ATGGTCAACGACCCTCCAGTACCTGC) and a 3′ primer (5′-BamHI-TCAGGAATTGTCTCTTTTTCGGATG) from human cDNA BC012140. The fragments were subcloned into SphI- and BamHI-cleaved or SphI- and XbaI-cleaved YCplac111-MET3 plasmid in which the MET3 promoter was inserted between HindIII and SphI restriction sites.

Site-directed mutagenesis. Site-directed mutagenesis was performed using the QuikChange II XL kit (Stratagene) according to the manufacturer's instructions.

Lipid analysis

Thin-layer chromatography and quantitation of neutral lipids. Lipid extraction from lyophilized yeast cells was performed as previously described (Zhang et al., 2003). In brief, cells were grown in the appropriate medium until the required growth phase (determined by OD_{600}), harvested, washed twice with 0.5% Nonidet P-40 and once with deionized H_2O, and lyophilized. The dried cell pellets were resuspended in 50 µl lyticase (Sigma-Aldrich) solution (1,700 U/ml in 10% glycerol) and incubated at 37°C for 15 min at −70°C for 1 h and at 37°C for 15 min. Lipids were extracted with hexane and blown dry. Quantitation of neutral lipids was performed as described previously by Zweytick et al. (2000) with modifications. Samples were dissolved in 100 µl chloroform/methanol (2:1; vol/vol) and applied to Silica gel 60 F_{254} plates (Merck), and chromatograms were developed in hexane/diethyl ether/acetic acid (85:15:1) with triolein and cholesteryl ester as the standard. For quantitation of SE and TAG, plates were dipped into methanolic $MnCl_2$ solution (0.63 g $MnCl_2$-$4H_2O$, 60 ml water, 60 ml methanol, and 4 ml of concentrated sulfuric acid), dried, and heated at 120°C for 15 min. Densitometric scanning was performed at 500 nm with a scanner (thin-layer chromatography; CAMAG). For each assay, at least three independent tests were performed; average and SD were calculated.

Oleic acid incorporation. Incorporation of [^{3}H]oleic acid into SE and TAG was performed as described previously (Zhang et al., 2003). 5 ml of cells at OD_{600} = ~0.6–0.8 were pulsed with 5 µCi [^{3}H]oleic acid at 30°C for 30 min with shaking. Lipid extraction and thin-layer chromatography were performed as mentioned in the previous paragraph except that the plates were stained with iodine vapor. Incorporation of label into neutral lipids was determined after scintillation counting (Beckman Coulter) and normalization to a [^{14}C]cholesterol internal standard and cell dry weight. For each assay, at least three independent tests were performed; average and SD were calculated.

Analysis of lipids using high performance liquid chromatography/mass spectrometry. A high performance liquid chromatography system (Agilent) coupled with a triple quadrupole/ion trap mass spectrometer (4000Qtrap; Applied Biosystems) was used for quantitation of individual lipids. Samples were introduced into the mass spectrometer by loop injections with chloroform/methanol/300 mM piperidine (1:1:0.1) as a mobile phase at a flow of 200 µl/min (Shui et al., 2007). Based on product ion and precursor ion analysis of head groups and fatty aclys, two comprehensive sets of multiple reaction monitoring (MRM) transitions were set up for quantitative analysis of various lipids (Guan et al., 2006), and results are expressed as normalized intensities.

Fatty acyl profiles of polar lipids. Fatty acyl profiles of polar lipids were acquired using a micromass spectrometer (Micromass Q-TOF; Waters Corp.) in the negative electrospray ionization ion mode. Piperidine (final concentration of 15 µM) was added into lipid extracts to enhance ionization (Leber et al., 1994). Samples were infused into the mass spectrometer at a flow rate of 15 µl/min. High collision energy (55 V) was applied to fragment polar lipid parent ions to generate fatty acyl profiles. The operation parameters for the mass spectrometer are a sample cone temperature of 250°C, a sample cone voltage of 70 V, and collision energy of 55 V. Mass spectra were recorded from mass/charge ratios of 140–900.

Calculation of lipid levels. Precursor ion or neutral loss scans of phospholipid headgroup fragments (Han and Gross, 2005) were used to obtain information on yeast phospholipid compositions. Based on this information, a comprehensive list of MRM transitions was set up to follow fatty acyl compositions of these lipids (parent→fatty acyl fragment transitions). The signal intensity of each MRM value was normalized using the following equation:

$$\text{Normalized intensity of lipid 1} = \frac{\text{Signal intensity of lipid 1}}{\sum \text{Signal intensity of all MRM transitions measured}}.$$

Cell fractionation

Preparation of spheroplasts. Cells were harvested by centrifugation at 3,000 *g* for 5 min, washed once with double-distilled H_2O, suspended to 0.5 g of wet weight/ml in 0.1 M Tris-Cl, pH 9.4, and 10 mM DTT, and incubated at 30°C for 10 min. Afterward, they were washed once with 1.2 M sorbitol and suspended in 1.2 M sorbitol and 20 mM K_3PO_4, pH 7.4, to 0.15 g of wet weight/ml. Zymose 20T was added to 2 mg/g of wet weight cells. The suspension was incubated at 30°C with gentle shaking for 20–60 min. Spheroplasts were harvested by centrifugation for 5 min at 1,500 *g*, washed twice with 1.2 M sorbitol, and suspended in the appropriate buffer for homogenization.

Differential centrifugation and sucrose density gradient analysis of whole cell extract. Spheroplasts were lysed in ice-cold lysis buffer II (50 mM Tris-HCl, pH 7.5, 1 mM EDTA, and 0.2 M sorbitol) containing protease inhibitors. Cell lysates were cleared at 500 *g* for 5 min, resulting in supernatant S5, which was then subjected to centrifugation at 13,000 *g* for 15 min, resulting in supernatant S13 and pellet P13. A continuous sucrose density gradient fractionation procedure was used as described previously (Kölling and Hollenberg, 1994) except that only 13 fractions were taken from top to bottom. In brief, cells were lysed in STED10 (10% wt/wt sucrose, 10 mM Tris, pH 7.4, 1 mM EDTA, and 1 mM DTT) using a glass bead beater and were spun at 500 *g* for 5 min to remove cell debris. 950 µl of cleared cell extract was loaded onto a sucrose density prepared as follows: in 13-ml centrifuge tubes (SW41; Beckman Coulter), 3.8 ml STED53 (53% sucrose), STED35 (35% sucrose), and STED20 (20% sucrose) was loaded on top of each other. Centrifugation was performed at 30,000 rpm for 13–17 h for membranes to reach their equilibrium density. 950-µl fractions were collected from the top of the gradient. Dpm1p was used as an ER marker.

Isolation of LDs. LDs were purified as described by Leber et al. (1994) with minor modifications. In brief, 0.15 g/ml spheroplasts were suspended in breaking buffer (10 mM Tris-Cl, pH 6.9, 0.2 mM EDTA, and 12% [wt/wt] Ficoll 400) and chilled on ice. Protease inhibitors were added in buffers as follows: 1 mM PMSF, 2 µg/ml aprotinin, 0.5 µg/ml leupeptine, and 1 µg/ml pepstatin A. Spheroplasts were homogenized with a Dounce homogenizer applying 10–20 strokes using a loose-fitting pestle, and the homogenate was transferred into 13.5-ml centrifuge tubes (Ultra-Clear; Beckman Coulter) and overlaid with an equal volume of breaking buffer. Centrifugation was performed for 60 min at 28,000 rpm in an SW41 swing bucket rotor (Beckman Coulter). A floating layer that consists mainly of LDs and vacuoles was collected and suspended gently in breaking buffer using a Dounce homogenizer with a loose-fitting pestle. The suspension was again transferred into 13.5-ml tubes, overlaid with an equal volume of 10 mM Tris-Cl, pH 7.4, 0.2 mM EDTA, and 8% (wt/wt) Ficoll 400, and centrifuged for 60 min at 28,000 rpm in an SW41 swing bucket rotor. The floating layer was recovered, suspended gently in 10 mM Tris-Cl, 0.2 mM EDTA, 0.6 M sorbitol, and 8% (wt/wt) Ficoll 400 in 13.5-ml tubes, and overlaid with 10 mM Tris-Cl, 0.2 mM EDTA, and 0.25 M sorbitol. After centrifugation at 28,000 rpm for 30 min, the floating layer consists of highly enriched LDs that are separated from vacuoles.

Online supplemental material

Tables S1 and S2 summarize the genes identified in the genome-wide screen for *fld* strains and *mld* strains, respectively. Fig. S1 presents neutral lipid analysis of wild-type and *ylr404wΔ* (*fld1Δ*) strains. Fig. S2 shows that mutants (*mld*) with increased levels of neutral lipids do not contain enlarged LDs. Fig. S3 is an analysis of phosphatidylethanolamine and phosphatidylcholine, which is continued from Fig. 5. Online supplemental material is available at http://www.jcb.org/cgi/content/full/jcb.200711136/DC1.

We thank Prof. Sepp Kohlwein for helpful discussions.

This work is jointly supported by research grants from the Biomedical Research Council of Singapore and the University of New South Wales to H. Yang as well as grants from the National Health and Medical Reasearch Council of Australia to R.G. Parton. The Institute for Molecular Bioscience is a special research center of the Australian Research Council. M.R. Wenk was supported by the Office of Life Sciences and the Academic Research Fund of the National University of Singapore and by the Biomedical Research Council of Singapore. L. Kuerschner is supported by a postdoctoral fellowship from the Deutsche Forschungsgemeinschaft.

Submitted: 27 November 2007
Accepted: 9 January 2008

References

Agarwal, A.K., and A. Garg. 2004. Seipin: a mysterious protein. *Trends Mol. Med.* 10:440–444.

Agarwal, A.K., E. Arioglu, S. De Almeida, N. Akkoc, S.I. Taylor, A.M. Bowcock, R.I. Barnes, and A. Garg. 2002. AGPAT2 is mutated in congenital generalized lipodystrophy linked to chromosome 9q34. *Nat. Genet.* 31:21–23.

Athenstaedt, K., and G. Daum. 2003. YMR313c/TGL3 encodes a novel triacylglycerol lipase located in lipid particles of *Saccharomyces cerevisiae*. *J. Biol. Chem.* 278:23317–23323.

Binns, D., T. Januszewski, Y. Chen, J. Hill, V.S. Markin, Y. Zhao, C. Gilpin, K.D. Chapman, R.G. Anderson, and J.M. Goodman. 2006. An intimate collaboration between peroxisomes and lipid bodies. *J. Cell Biol.* 173:719–731.

Bostrom, P., M. Rutberg, J. Ericsson, P. Holmdahl, L. Andersson, M.A. Frohman, J. Boren, and S.O. Olofsson. 2005. Cytosolic lipid droplets increase in size by microtubule-dependent complex formation. *Arterioscler. Thromb. Vasc. Biol.* 25:1945–1951.

Bostrom, P., L. Andersson, M. Rutberg, J. Perman, U. Lidberg, B.R. Johansson, J. Fernandez-Rodriguez, J. Ericson, T. Nilsson, J. Borén, and S.O. Olofsson. 2007. SNARE proteins mediate fusion between cytosolic lipid droplets and are implicated in insulin sensitivity. *Nat. Cell Biol.* 9:1286–1293.

Gale, S.E., A. Frolov, X. Han, P.E. Bickel, L. Cao, A. Bowcock, J.E. Schaffer, and D.S. Ory. 2006. A regulatory role for 1-acylglycerol-3-phosphate-O-acyltransferase 2 in adipocyte differentiation. *J. Biol. Chem.* 281:11082–11089.

Greenspan, P., E.P. Mayer, and S.D. Fowler. 1985. Nile red: a selective fluorescent stain for intracellular lipid droplets. *J. Cell Biol.* 100:965–973.

Guan, X.L., X. He, W.Y. Ong, W.K. Yeo, G. Shui, and M.R. Wenk. 2006. Nontargeted profiling of lipids during kainate-induced neuronal injury. *FASEB J.* 20:1152–1161.

Han, G.S., W.I. Wu, and G.M. Carman. 2006. The *Saccharomyces cerevisiae* Lipin homolog is a Mg2+-dependent phosphatidate phosphatase enzyme. *J. Biol. Chem.* 281:9210–9218.

Han, X., and R.W. Gross. 2005. Shotgun lipidomics: electrospray ionization mass spectrometric analysis and quantitation of cellular lipidomes directly from crude extracts of biological samples. *Mass Spectrom. Rev.* 24:367–412.

Kaiser, C., S. Michaelis, and A. Mitchell. 1994. Methods in Yeast Genetics: a Cold Spring Harbor Laboratory Course Manual. Cold Spring Harbor Laboratory, Cold Spring Harbor, NY. 234 pp.

Kölling, R., and C.P. Hollenberg. 1994. The ABC-transporter Ste6 accumulates in the plasma membrane in a ubiquitinated form in endocytosis mutants. *EMBO J.* 13:3261–3271.

Leber, R., E. Zinser, G. Zellnig, F. Paltauf, and G. Daum. 1994. Characterization of lipid particles of the yeast, *Saccharomyces cerevisiae*. *Yeast.* 10:1421–1428.

Lundin, C., R. Nordstrom, K. Wagner, C. Windpassinger, H. Andersson, G. von Heijne, and I. Nilsson. 2006. Membrane topology of the human seipin protein. *FEBS Lett.* 580:2281–2284.

Magre, J., M. Delepine, E. Khallouf, T. Gedde-Dahl Jr., L. Van Maldergem, E. Sobel, J. Papp, M. Meier, A. Megarbane, A. Bachy, et al. 2001. Identification of the gene altered in Berardinelli-Seip congenital lipodystrophy on chromosome 11q13. *Nat. Genet.* 28:365–370.

Martin, S., and R.G. Parton. 2006. Lipid droplets: a unified view of a dynamic organelle. *Nat. Rev. Mol. Cell Biol.* 7:373–378.

Martin, S., K. Driessen, S.J. Nixon, M. Zerial, and R.G. Parton. 2005. Regulated localization of Rab18 to lipid droplets: effects of lipolytic stimulation and inhibition of lipid droplet catabolism. *J. Biol. Chem.* 280:42325–42335.

McGuffin, L.J., K. Bryson, and D.T. Jones. 2000. The PSIPRED protein structure prediction server. *Bioinformatics.* 16:404–405.

Murphy, D.J., and J. Vance. 1999. Mechanisms of lipid-body formation. *Trends Biochem. Sci.* 24:109–115.

Oelkers, P., D. Cromley, M. Padamsee, J.T. Billheimer, and S.L. Sturley. 2002. The DGA1 gene determines a second triglyceride synthetic pathway in yeast. *J. Biol. Chem.* 277:8877–8881.

Shui, G., A.K. Bendt, K. Pethe, T. Dick, and M.R. Wenk. 2007. Sensitive profiling of chemically diverse bioactive lipids. *J. Lipid Res.* 48:1976–1984.

Simossis, V.A., and J. Heringa. 2005. PRALINE: a multiple sequence alignment toolbox that integrates homology-extended and secondary structure information. *Nucleic Acids Res.* 33:W289–W294.

Windpassinger, C., M. Auer-Grumbach, J. Irobi, H. Patel, E. Petek, G. Horl, R. Malli, J.A. Reed, I. Dierick, N. Verpoorten, et al. 2004. Heterozygous missense mutations in BSCL2 are associated with distal hereditary motor neuropathy and Silver syndrome. *Nat. Genet.* 36:271–276.

Winzeler, E.A., D.D. Shoemaker, A. Astromoff, H. Liang, K. Anderson, B. Andre, R. Bangham, R. Benito, J.D. Boeke, H. Bussey, et al. 1999. Functional characterization of the *S. cerevisiae* genome by gene deletion and parallel analysis. *Science.* 285:901–906.

Wolins, N.E., D.L. Brasaemle, and P.E. Bickel. 2006. A proposed model of fat packaging by exchangeable lipid droplet proteins. *FEBS Lett.* 580:5484–5491.

Zhang, Q., H.K. Chieu, C.P. Low, S. Zhang, C.K. Heng, and H. Yang. 2003. *Schizosaccharomyces pombe* cells deficient in triacylglycerols synthesis undergo apoptosis upon entry into the stationary phase. *J. Biol. Chem.* 278:47145–47155.

Zweytick, D., E. Leitner, S.D. Kohlwein, C. Yu, J. Rothblatt, and G. Daum. 2000. Contribution of Are1p and Are2p to steryl ester synthesis in the yeast *Saccharomyces cerevisiae*. *Eur. J. Biochem.* 267:1075–1082.